

Superlenses to overcome the diffraction limit

The imaging resolution of conventional lenses is limited by diffraction. Artificially engineered metamaterials now offer the possibility of building a superlens that overcomes this limit. We review the physics of such superlenses and the theoretical and experimental progress in this rapidly developing field. Superlenses have great potential in applications such as biomedical imaging, optical lithography and data storage.

XIANG ZHANG AND ZHAOWEI LIU

5130 Etcheverry Hall, Nanoscale Science and Engineering Center, University of California, Berkeley, California 94720–1740, USA

e-mail: xiang@berkeley.edu

Making a perfect lens that produces flawless images has been a dream of lens makers for centuries. In 1873, Ernst Abbe discovered a fundamental ‘diffraction limit’ in optics: whenever an object is imaged by an optical system, such as the lens of a camera, fine features — those smaller than half the wavelength of the light — are permanently lost in the image. The loss of information arises because light emerging from the object’s fine features carries components with high spatial frequency — that is, evanescent waves that exponentially decay, resulting in an imperfect image. The ‘lost treasures’, as the subwavelength details could be called, are the fundamental reason for Abbe’s diffraction limit, which determines the smallest features that one can see through even the best of lenses. Practically speaking, this limits the resolution of all the imaging and lithography systems that are the corner stones of modern biology and electronics.

For more than a century, attempts have been made to overcome the diffraction limit. In 1967, Veselago raised the question of the physical meaning and feasibility of hypothetical materials with a negative index of refraction. He found that in such negative index media (NIM) a number of surprising phenomena occur, such as the reverse equivalents of Snell’s law, Doppler shift and Cerenkov radiation¹. These new phenomena do not violate the laws of physics, yet they challenge our physical perception and intuition. Negative refraction at the interface of a negative and a positive index medium allows a flat slab of NIM to focus all the diverging light rays from an object into two images: one inside the slab and one outside (Fig. 1a).

The idea of the NIM lens remained obscure for some decades, primarily because no such materials exist in nature. To achieve a negative index, a material must simultaneously possess a negative dielectric permittivity ϵ and a negative magnetic permeability μ . Although the dielectric resonances that lead to negative ϵ do occur in nature at optical frequencies in noble metals, the magnetic resonances typically dissipate above 100 GHz. Attempts to adjust the two resonance frequencies supported by the same material to match each other, such as in magnetic semiconductors, has proven nearly impossible. In the late 1990s, Pendry proposed that electromagnetic resonances in artificially engineered metamaterials made of metal loops and wires could be tuned to values not accessible in natural materials^{2,3}. By regulating these artificial ‘meta-atoms’, which are much smaller than the working wavelength, the electric and magnetic

resonances could be tailored individually and made to overlap at a desired frequency^{4,5}. The first NIM was experimentally demonstrated in 2000 at microwave frequencies^{6,7} (~10 GHz). The metamaterial’s construction was a cubic lattice of artificial meta-atoms with splitting resonators, providing the negative μ , and metallic wires that mimic a diluted metal below its plasma frequency, providing the negative ϵ . This type of microwave NIM was further confirmed by other groups^{8–10} and can now be routinely produced.

One of the most striking properties of NIM materials, further proposed by Pendry, is that a slab of NIM can be a ‘perfect lens’ in which the evanescent waves, instead of decaying, are in fact enhanced through the slab¹¹. This offers the possibility of restoring or recovering the ‘lost treasures’, theoretically making a perfect image without any deterioration. These bold and provocative theoretical predictions have renewed hopes of overcoming the diffraction limit. In the past few years, we have witnessed exciting theoretical and experimental steps towards the realization of such lenses (Box 1). These new developments not only demonstrate the physics of the concept, but also pave the way for future optical and photonic applications.

PHYSICS OF THE SUPERLENS

The light emitted or scattered from an object includes not only propagating waves but also evanescent waves, which carry the subwavelength detail of the object. The evanescent waves decay exponentially in any medium with a positive refractive index so that they cannot be collected at the image plane by a conventional lens, and this results in a diffraction-limited image. But if a lens made of NIM is placed close to an object, the near-field evanescent waves can be strongly enhanced across the lens¹¹ (Fig. 1b). After emerging from the NIM lens, the evanescent waves decay again until their amplitudes reach their original level at the image plane. On the other hand, the propagating waves pass through the NIM lens with both negative refraction and a reversed phase front, leading to zero phase change at the image plane. By completely recovering both propagating and evanescent waves in phase and amplitude, a perfect image is created (see Fig. 1c).

Such intriguing behaviour relies on the fact that the NIM supports resonant surface waves, one example of which is surface plasmon polaritons. Evanescent waves can be efficiently coupled into surface modes and enhanced by their resonant nature when their wave vectors are matched. Because the amplitude of the coupled evanescent waves measures the stored energy in the material, the

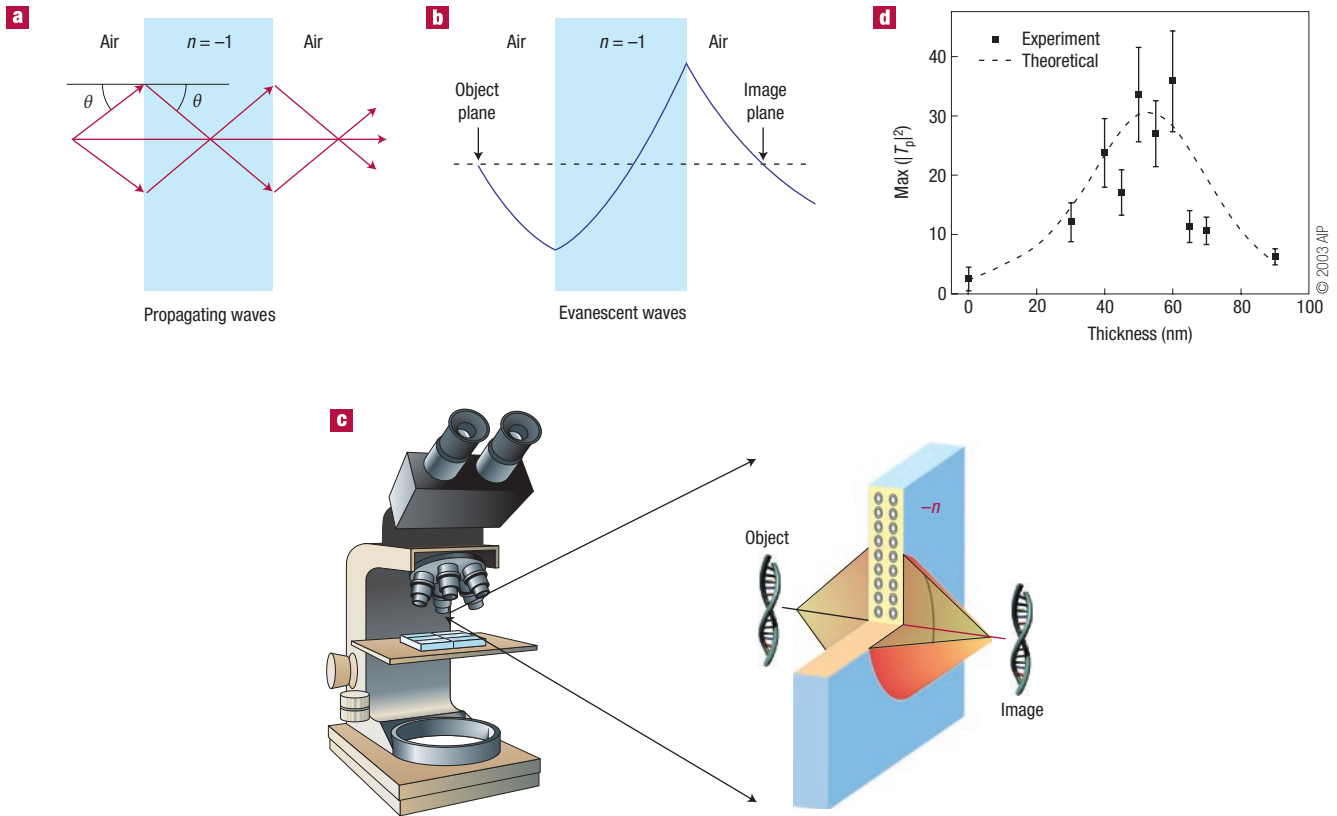


Figure 1 A slab of negative-refractive-index medium acts as a perfect lens. **a**, A NIM flat lens brings all the diverging rays from an object into a focused image. **b**, The NIM can also enhance the evanescent waves across the lens, so the amplitude of the evanescent waves are identical at the object and the image plane. **c**, A microscope based on an ideal NIM lens should focus both propagating and evanescent waves into an image with arbitrarily high resolution. **d**, Experimental verification of the evanescent wave enhancement through a silver superlens. T_p is the enhancement factor. Reprinted with permission from ref. 16.

enhancement can be built up by a few cycles of electromagnetic oscillations in the surface resonance. Because the evanescent waves do not carry any net energy flux, the energy can never be amplified; only the distribution of the energy or field will be modified across the space. Resonance-based negative-refractive-index media constructed from realistic materials, however, are inherently associated with substantial energy dissipation or loss (that is, the imaginary part of ϵ and μ), which hinders the resolution of the ‘perfect image’. The term ‘superlens’ is used for lenses that take this practical limit into account. Unlike conventional lenses, the resolution of the superlens is not limited by diffraction, but rather determined by the enhancement and by how many evanescent modes can be restored. Another consequence of the material loss and imperfections is that the distance between the slab and both the object and its image, as well as the slab’s thickness, must all be small compared with the wavelength if we are to obtain meaningful resonant enhancement of the evanescent waves¹². When their scale is deeply subwavelength, the electrostatic limit can be applied. In this case, the electric and magnetic responses of a material decouple, and only one material property (ϵ or μ) needs to be negative to support resonant surface waves for one specific polarization (transverse magnetic, TM, or transverse electric, TE mode)¹¹. In this special case, the superlens effect therefore remains valid in a single negative index medium for one polarization of light. As a natural candidate having negative ϵ at optical frequencies, a slab of silver (because of low loss in metal) was suggested for achieving the superlens effect for TM waves in optics¹¹. Detailed theoretical studies on superlens properties have

since been extensively explored in terms of resolution, inherent loss, dielectric mismatch and also geometrical optimizations^{12–15}.

SUPERLENSING IN THE NEAR FIELD

Soon after Pendry’s theoretical proposal, experimental attempts to test the superlens concept began. The key feature needed in a superlens is its ability to enhance the evanescent waves, resulting in a sharper image. In 2003, an optical experiment demonstrated that evanescent waves are indeed significantly enhanced across a silver slab (Fig. 1d)^{16,17}. The experiment found that the evanescent enhancement factor increases exponentially until a particular film thickness when the material loss becomes more prominent. This experiment not only confirmed the evanescent enhancement mechanism in Pendry’s theory, but also provided a number of suggestions, such as optimized film thickness and surface roughness requirements, for experimental demonstration of a superlens. Subsequently, the evanescent enhancement was also observed in negative-index and negative- μ metamaterials at microwave frequencies^{18,19}.

Superlenses have been realized in both microwave^{18,20,21} and optical frequencies^{22–24} but with different designs. A microwave metamaterial was constructed from wires and split-ring resonators forming a two-dimensional waveguide that can be treated as homogeneous because the 3-centimetre wavelength is much larger than the lattice constant²⁰. With an input antenna placed 2 centimetres away from a rectangular slab of metamaterial, a focused image was

Box 1 Superlenses and hyperlenses

When a beam of light hits an object, the object's information is transferred to the scattered light with various wave vectors which comprise both propagating and evanescent components. The propagating waves carry large feature information and can reach the far field, whereas evanescent waves carry fine details, but are confined to the near field. If a conventional glass lens is used to collect the scattered light, the evanescent waves are permanently lost before reaching the image plane (Fig. B1a). Thus, the resolution of the final image is always 'diffraction limited'.

However, the evanescent fields can be enhanced and thus contribute to a sub-diffraction-limited image if we place a superlens with negative refractive index close to the object (Fig. B1b). If the superlens only possesses either single negative ϵ or single negative μ , the superlens effect remains valid only for transverse magnetic or transverse electric modes of light, respectively.

By adding a coupling element to the superlens, the enhanced evanescent waves can be coupled into propagating waves, making far-field detection possible (Fig. B1c). High-resolution images can be reconstructed by collecting the far-field signals from such a lens if we have complete knowledge of the coupling process, which is assured by the design of the FSL transfer function.

Taking another approach, the hyperlens uses a piece of artificial metamaterial to transfer the deep subwavelength information into the far field (Fig. B1d). The evanescent waves from the object can become propagating waves in such a strongly anisotropic metamaterial. With the help of the hyperlens geometry, the waves gradually reduce their wavevector values along the propagation direction in the metamaterial, and thus the waves can continue to propagate even after leaving the hyperlens.

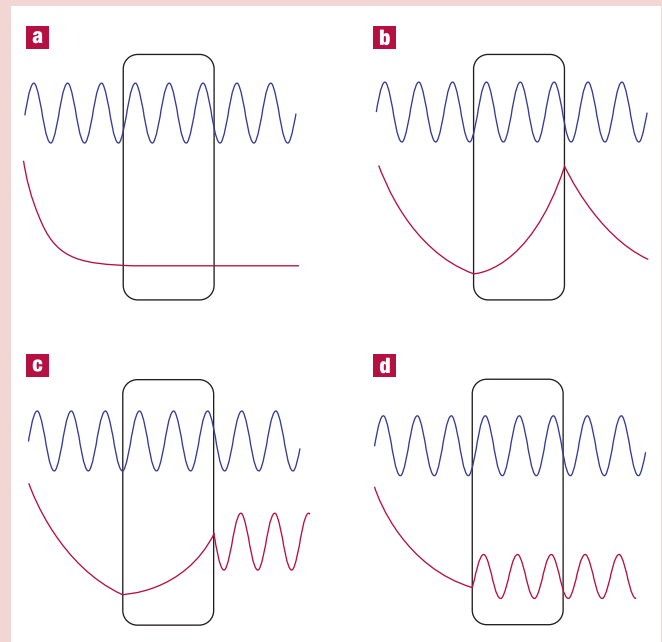


Figure B1 Comparison of various types of optical lenses. **a**, Conventional lens. **b**, Near-field superlens. **c**, Far-field superlens. **d**, Hyperlens. The wavy curves and smooth curves represent propagating waves and evanescent waves, respectively.

obtained by scanning the detector on the imaging side of the sample. By using a negative-index planar transmission-line structure, an image below the diffraction limit (at $\lambda/5$) was reported at ~ 1 GHz frequency¹⁸. Although these metamaterials experienced significant loss and are very sensitive to frequency and their electromagnetic environment, the experimental results demonstrated the superlens effect in the microwave range.

In 2005, the optical superlensing effect was observed using a thin slab of silver, a single negative- ϵ material, that could effectively image 60-nm features ($\lambda/6$), well below the diffraction limit^{22,23}. The sub-diffraction-limited image was recorded by optical lithography at 365 nm wavelength as shown in Fig. 2a–c. The presence of the silver superlens improved the image resolution remarkably in the near field by excitation of surface plasmons. Using a similar scheme, another group also confirmed the superlensing effect in silver films²⁴. The concept of the basic single-layer silver superlens was also improved by lamination of the metal into many layers^{25–28}. A year later, a SiC superlens at mid-infrared frequency, using optical phonon resonance enhancement, showed even better feature resolution in terms of wavelength ($\lambda/20$) because of the low loss in the SiC material²⁹. Despite challenges in fabricating ultra-flat surfaces on either side of the superlens (surfaces roughness being detrimental to the surface resonances and enhancement), these experimental realizations of the optical superlens clearly showed the potential for imaging and lithography below the diffraction limit.

Negative refraction and imaging in photonic crystals have also come in for intensive investigation^{30–40}. Using low-loss dielectric materials, this can be an interesting approach to counter the loss that NIM must deal with. The key to the superlens effect in photonic crystals is to design appropriate dispersion so as to achieve negative

refraction for all angles. Although the lensing effect is similar to the NIM case, it arises from a different mechanism: Bragg scattering in a photonic crystal rather than refraction in NIM. The ultimate image resolution therefore is limited by the period of the crystal, and the image contains some distortions as well, because the evanescent components cannot be uniformly enhanced by the surface mode for all wave vectors³².

SUPERLENSES PROJECTING FAR-FIELD IMAGES

The superlens experiments discussed so far are only capable of projecting a sub-diffraction-limited image in the near field, as the evanescent waves will continue to decay away from such lenses. A simple slab superlens is 'near-sighted'^{11,41}. How to bring the image into the far field remains a substantial challenge. In this section, we discuss a few recent approaches towards this goal.

FAR-FIELD SUPERLENS

A silver superlens-based device, termed the far-field superlens (FSL), was proposed to project a sub-diffraction-resolution image into the far field⁴². The FSL is made of a silver superlens with additional nanoscale corrugations on its top surface (Fig. 3a). This lens not only enhances the evanescent waves but also converts them into propagating waves. A proper transfer function of the FSL is crucial, because it ensures the 'uniqueness' required for the reconstruction process to form sub-diffraction-limit images. The concept was first tested with a carefully designed silver FSL geometry working at 377 nm wavelength^{43,44}. After inserting the FSL into a conventional optical microscope, two nanowires of 50 nm width separated by a 70-nm gap were clearly imaged (Fig. 3b,d). As a comparison,

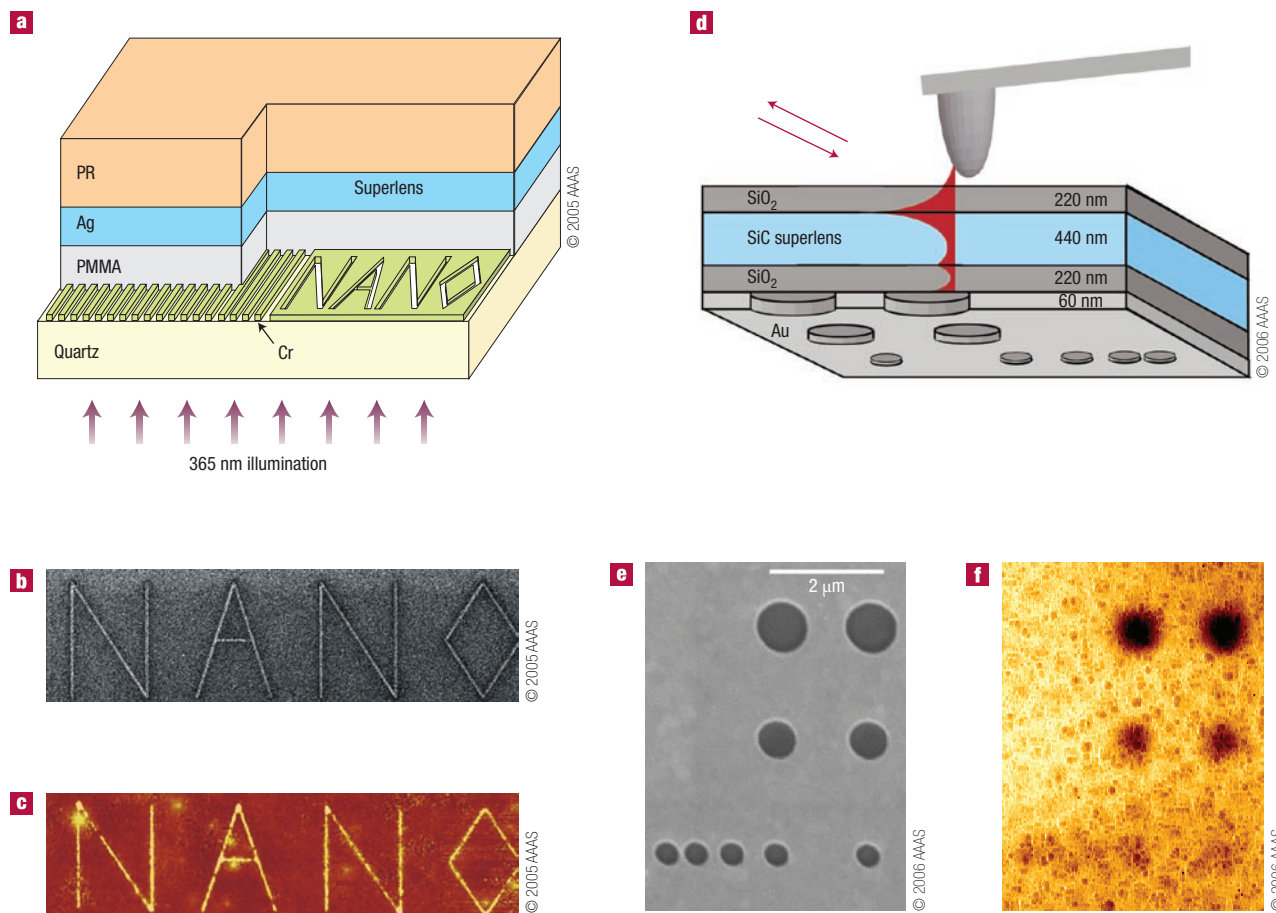


Figure 2 Near-field optical superlenses. **a**, Schematic configuration for the silver superlens experiment. PR, photoresist layer; PMMA, polymethylmethacrylate. The superlens image was revealed by means of photolithography at wavelength $\lambda = 365$ nm. **b**, Focused ion-beam image of the object with a 40-nm linewidth. **c**, Atomic force microscopy of the developed image on photoresist with a silver superlens. The presence of the superlens improved the resolution to 89 nm from an average linewidth of $321 \pm 10 \text{ nm}$ without the superlens. **d**, Schematic configuration for the SiC superlens experiment. The image transferred through the superlens was recorded by near-field scanning microscopy. **e**, Scanning electron microscope (SEM) image of the object. Scale bar, $2 \mu\text{m}$. **f**, Amplitude image through the SiC superlens measured by near-field scanning microscopy at $\lambda = 10.85 \mu\text{m}$. **a–c**, Reprinted with permission from ref. 22. **d–f**, Reprinted with permission from ref. 29.

without the FSL, the same optical microscope cannot resolve the details of such nanostructures (Fig. 3c).

A tunable FSL capable of working at any visible wavelength was recently investigated (Fig. 3e)^{45,46}. The silver slab in the original design was replaced by a slab of silver dielectric multilayers. The mechanism of evanescent wave enhancement for a broad range of wave vectors comes from a well-known surface plasmon mode splitting, so that a multilayer-based FSL can be designed to work at any frequency below the surface plasmon frequency⁴⁶. Similar multilayer structures without coupling elements have been used for near-field superlenses^{25–28}, but the working wavelength has to be close to the surface plasmon frequency and the bandwidth is rather narrow. Numerical calculations showed that a two-dimensional arbitrary particle of 40 nm radius can be imaged with sub-diffraction-limited resolution by a multilayer FSL (see Fig. 3f; ref. 46). Although these results are encouraging, experimental challenges remain.

THE HYPERLENS AS AN OPTICAL TURBINE

The FSL obtains a sub-diffraction-limited image in the far field using a two-stage process: evanescent wave enhancement via surface resonance, and subsequently, conversion into a propagation wave at the exit surface via a designed surface scatterer.

An alternative approach uses an anisotropic medium in curved multilayer stacks. The evanescent waves can tunnel through flat films to produce a high-resolution image^{25–28}. However, the image exists only at the near field of the final layer. In 2006, two groups^{47,48} independently proposed that an anisotropic metamaterial with hyperbolic dispersion (see Fig. 4a) could provide magnification in a cylindrical geometry. When ordinary evanescent waves enter such anisotropic media, they immediately become propagating. What is interesting is that their large transverse wave vectors can be gradually compressed as they propagate outwards, until they are small enough to be truly propagating in air or surrounding dielectrics outside this cylindrical medium, projecting a magnified image into the far field. The cylindrical anisotropic lens has been termed a ‘hyperlens’ because of the hyperbolic function of the dispersion in such a metamaterial. Practically, the hyperbolic curve in Fig. 4a needs to be designed to be nearly flat so that the waves with different transverse wave vectors will all propagate with the same phase velocity along the radial direction, which is important in forming an undistorted image in the far field⁴⁹. The hyperlens essentially works as an optical compressor or turbine that continuously compresses or transforms the large wave vectors of the original evanescent waves into smaller ones that propagate

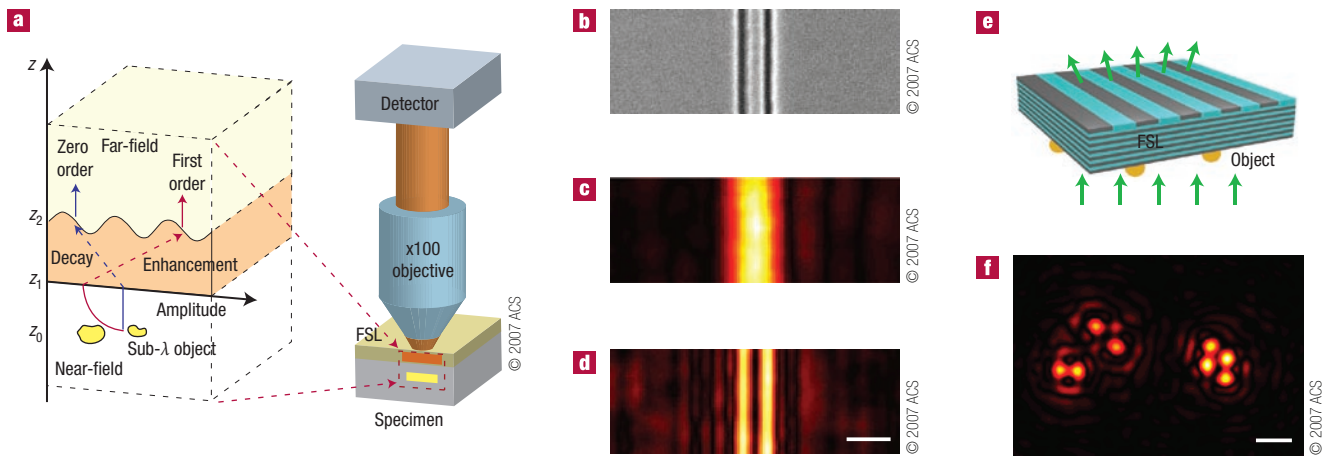


Figure 3 Far-field optical superlens. **a**, A far-field superlens is constructed by adding a subwavelength grating onto a silver slab superlens. It can selectively enhance the evanescent waves from the object and also convert them into propagating waves. An FSL microscope can be produced by inserting an FSL between the specimen and objective lens of a regular microscope. **b**, SEM image of a nanowire pair object with 50-nm-wide slit in Cr film separated by a 70-nm gap. **c**, Diffraction-limited image from a regular microscope cannot resolve the two nanowires (numerical aperture = 1.4, $\lambda = 377$ nm). **d**, Reconstructed FSL image clearly resolves the sub-diffraction details at $\lambda = 377$ nm. Scale bar, 200 nm. **e**, A new generation of FSL in which the original silver slab is replaced by a silver–dielectric multilayer structure so that the lens works at visible wavelengths. **f**, A numerical demonstration of two-dimensional sub-diffraction-limited imaging at 405 nm wavelength using the multilayer FSL. The image was reconstructed by collecting signals in the far field from six different FSL grating orientations. The object consists of particles with a 40-nm radius and 100-nm smallest centre-to-centre distance. Scale bar, 200 nm. **a–d**, Reprinted with permission from ref. 43. **f**, Reprinted with permission from ref. 46.

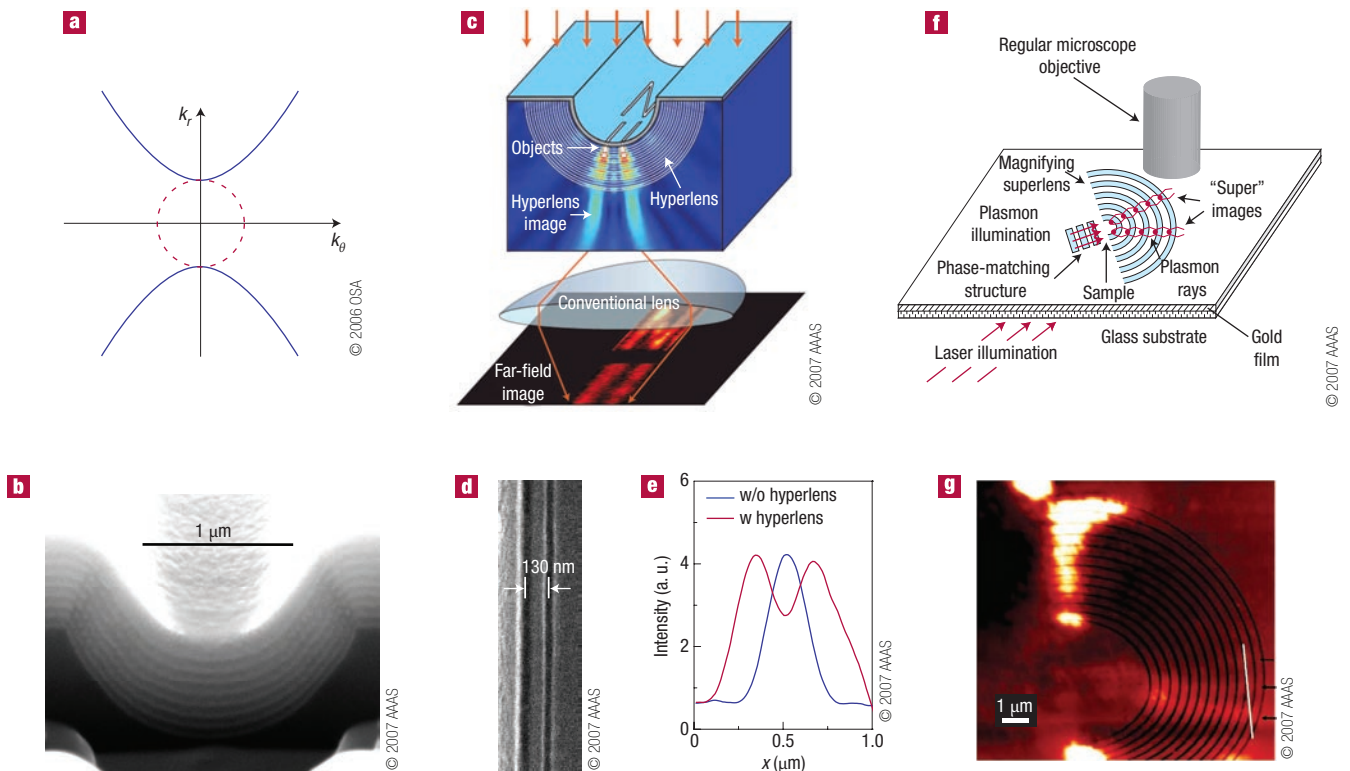


Figure 4 Optical hyperlens and magnifying superlens. **a**, For a material with $\epsilon_r < 0$, $\epsilon_i > 0$, the k_x and k_y relationship shows a hyperbolic curve. The propagating waves in such medium can take on arbitrarily large values of k_y . Reprinted with permission from ref. 47. **b**, SEM image of the cross-section of a hyperlens made by depositing 16 periodic silver (35 nm) and Al_2O_3 (35 nm) layers on a cylindrical cavity in quartz substrate. Reprinted with permission from ref. 52. **c**, Schematic of the experimental set-up for the first hyperlens demonstration. Reprinted with permission from ref. 52. **d**, SEM image of the pair object (the two dark lines) with 50-nm linewidths separated by an 80-nm gap. **e**, Comparison of the far-field image with and without the hyperlens, both at $\lambda = 365$ nm. The magnification of the hyperlens is about 2.3. **f**, Schematic of the magnifying superlens for surface plasmons. The lateral distance between the images produced by the alternating layers of effective negative refractive index grows with distance along the radius. The magnified images are scattered by the surface roughness and captured by a regular microscope. **g**, Composite of the atomic force microscope image of the sample and the corresponding image obtained by regular microscopy. **f, g**, Reprinted with permission from ref. 53.

to the far field. A similar cylindrical magnifying superlens was proposed by Pendry several years earlier^{50,51}.

The first optical hyperlens was successfully created by conformal film deposition of alternating Ag and Al₂O₃ thin films on a pre-fabricated quartz substrate moulded with a cylindrical cavity (see cross-section scanning electron micrograph in Fig. 4b)^{49,52}. On combining such a hyperlens with a conventional optical microscope, an image with 130-nm resolution, well below the diffraction limit of 260 nm, was directly observed in the far field (Fig. 4c–e). In addition to the magnification in one dimension shown in this work, a two-dimensional hyperlens is possible with a spherical geometry. A different approach to making a magnifying superlens used two-dimensional surface plasmon waves confined by a concentric polymer grating placed on a metal surface (see Fig. 4f)^{53,54}. The magnified images of the surface waves were scattered by the surface roughness and collected by a microscope (Fig. 4g).

Although the magnification of hyperlenses in these proof-of-concept experiments is moderate (2–3 times), the ultimate resolution has yet to be achieved. This is essentially determined by the geometry, material loss and quality of fabrication. For a hyperlens, the resolution could be further improved at least several times by increasing the ratio of the outer to inner radii and by using thinner films, but at the expense of a smaller field of view and a reduced total transmission. On the other hand, although an FSL does not have the limitation of a small imaging area, its magnification is dependant on the coupling grating and the bandwidth for propagating waves. To obtain the very large bandwidth in Fourier space needed to reconstruct a deep sub-diffractive image, the information might have to be collected from multiple measurements.

OUTLOOK

The superlens, with its unique ability to overcome the diffraction barrier, has vast potential for future applications. Over the past few years, we have witnessed some breakthroughs in demonstration of the superlensing effect, yet there remain considerable practical challenges. The chief limitation of present designs of the far-field superlens or hyperlens is that the object must be in the near field of the superlens, although the image can be projected into the far field. This is because one has to make sure that the evanescent waves do not decay too much before reaching the superlens and being enhanced or converted into propagating waves. An entirely new approach to this issue may be needed, although practical applications are still possible with the object near the lens. Another fundamental challenge is the loss, as most superlens schemes involve resonances in metal, which limits both the practical resolution and transmission. Imperfect sample fabrication further aggravates the performances because small perturbations are often strong enough to distort the delicate transformations of large wave vectors.

The quest for materials with truly negative index at optical frequencies presents the possibility of building an optical superlens for both polarizations. However, one may question whether this direction is better than single negative metamaterials in terms of losses, simplicity of design and fabrication. Recently, there have been a few interesting experiments showing the feasibility of achieving a negative index in a monolayer of metamaterials^{55–60}. It has yet to be seen in bulk optical metamaterials, where a truly negative refractive index can be defined, even though the ultimate resolution in metamaterials is still limited by the unit size of the meta-atom. Acoustic metamaterials are another emerging topic: negative density⁶¹ and negative modulus⁶² have been observed experimentally and various phenomena have been studied^{63–67}. We anticipate that an acoustic superlens will be realized experimentally in the not too distant future, and that this could greatly improve underwater sonar sensing and ultrasonic imaging for medical diagnostics.

In many areas of science and technology, the superlens has exciting potential. A possible futuristic optical nanoscope using superlenses may extend the optical microscope into the nanometre scale, with similar impact to the way in which optical microscopy transformed modern biology. Although there are currently quite a few imaging technologies, such as scanning electron microscopy, that offer nanometre resolution, an optical nanoscope is essential for real-time *in situ* observation of complex molecular machinery in living biological cells, which will accelerate discoveries in biology and medicine. Another possible application is the extension of optical lithography to ultra-small scales, which is the key to scaling down integrated circuits for high-performance electronics. Optical and magnetic data storage, and biosensing⁶⁸ may also benefit from the ability to write or read information within ultra-small volume, thereby increasing storage densities or sensing resolution.

doi:10.1038/nmat2141

References

- Veselago, V. G. The electrodynamics of substances with simultaneously negative values of ϵ and μ . *Sov. Phys. Uspekhi-USSR* **10**, 509–514 (1968).
- Pendry, J. B. *et al.* Extremely low frequency plasmons in metallic mesostructures. *Phys. Rev. Lett.* **76**, 4773–4776 (1996).
- Pendry, J. B. *et al.* Magnetism from conductors and enhanced nonlinear phenomena. *IEEE Trans. Microwave Theory Tech.* **47**, 2075–2084 (1999).
- Soukoulis, C. M., Linden, S. & Wegener, M. Negative refractive index at optical wavelengths. *Science* **315**, 47–49 (2007).
- Shalaev, V. M. Optical negative-index metamaterials. *Nature Photon.* **1**, 41–48 (2007).
- Smith, D. R. *et al.* Composite medium with simultaneously negative permeability and permittivity. *Phys. Rev. Lett.* **84**, 4184–4187 (2003).
- Shelby, R. A., Smith, D. R. & Schultz, S. Experimental verification of a negative index of refraction. *Science* **292**, 77–79 (2001).
- Bayindir, M. *et al.* Transmission properties of composite metamaterials in free space. *Appl. Phys. Lett.* **81**, 120–122 (2002).
- Parazzoli, C. G. *et al.* Experimental verification and simulation of negative index of refraction using Snell's Law. *Phys. Rev. Lett.* **90**, 107401 (2003).
- Gregor, R. B., Parazzoli, C. G. & Tanielian, M. H. Origin of dissipative losses in negative index of refraction materials. *Appl. Phys. Lett.* **82**, 2356–2358 (2003).
- Pendry, J. B. Negative refraction makes a perfect lens. *Phys. Rev. Lett.* **85**, 3966–3969 (2000).
- Smith, D. R. *et al.* Limitations on subdiffraction imaging with a negative refractive index slab. *Appl. Phys. Lett.* **82**, 1506–1508 (2003).
- Fang, N. & Zhang, X. Imaging properties of a metamaterial superlens. *Appl. Phys. Lett.* **82**, 161–163 (2003).
- Podolskiy, V. A. Optimizing the superlens: manipulating geometry to enhance the resolution. *Appl. Phys. Lett.* **87**, 231113 (2005).
- Larkin, I. A. & Stockman, M. I. Imperfect perfect lens. *Nano Lett.* **5**, 339–343 (2005).
- Liu, Z. *et al.* Rapid growth of evanescent wave with a silver superlens. *Appl. Phys. Lett.* **83**, 5184–5186 (2003).
- Fang, N., Liu, Z., Yen, T. J. & Zhang, X. Regenerating evanescent waves from a silver superlens. *Opt. Express* **11**, 682–687 (2003).
- Grbic, A. & Eleftheriades, G. V. Overcoming the diffraction limit with a planar left-handed transmission-line lens. *Phys. Rev. Lett.* **92**, 117403 (2004).
- Popa, B. I. & Cummer, S. A. Direct measurement of evanescent wave enhancement inside passive metamaterials. *Phys. Rev. E* **73**, 016617 (2006).
- Houck, A. A., Brock, J. B. & Chuang, I. L. Experimental observations of a left-handed material that obeys Snell's law. *Phys. Rev. Lett.* **90**, 137401 (2003).
- Lagarkov, A. N. & Kissel, V. N. Near-perfect imaging in a focusing system based on a left-handed-material plate. *Phys. Rev. Lett.* **92**, 077401 (2004).
- Fang, N. *et al.* Sub-diffraction-limited optical imaging with a silver superlens. *Science* **308**, 534–537 (2005).
- Lee, H. *et al.* Realization of optical superlens imaging below the diffraction limit. *New J. Phys.* **7**, 255 (2005).
- Melville, D. & Blaikie, R. Super-resolution imaging through a planar silver layer. *Opt. Express* **13**, 2127–2134 (2005).
- Shamonina, E. *et al.* Imaging, compression and Poynting vector streamlines for negative permittivity materials. *Electron. Lett.* **37**, 1243–1244 (2001).
- Ramakrishna, S. A. *et al.* Imaging the near field. *J. Mod. Opt.* **50**, 1419–1430 (2003).
- Belov, P. A. & Hao, Y. Subwavelength imaging at optical frequencies using a transmission device formed by a periodic layered metal-dielectric structure operating in the canalization regime. *Phys. Rev. B* **73**, 113110 (2006).
- Wood, B., Pendry, J. B. & Tsai, D. P. Directed subwavelength imaging using a layered metal-dielectric system. *Phys. Rev. B* **74**, 115116 (2006).
- Taubner, T. *et al.* Near-field microscopy through a SiC superlens. *Science* **313**, 1595 (2006).
- Notomi, M. Theory of light propagation in strongly modulated photonic crystals: refractionlike behavior in the vicinity of the photonic band gap. *Phys. Rev. B* **62**, 10696–10705 (2000).
- Luo, C. *et al.* All-angle negative refraction without negative effective index. *Phys. Rev. B* **65**, 201104 (2002).
- Luo, C. *et al.* Subwavelength imaging in photonic crystal. *Phys. Rev. B* **68**, 045115 (2003).

33. Efros, A. L. & Pokrovsky, A. L. Dielectric photonic crystal as medium with negative electric permittivity and magnetic permeability. *Solid State Commun.* **129**, 643–649 (2004).
34. Foteinopoulou, S. & Soukoulis, C. M. Negative refraction and left-handed behavior in two-dimensional photonic crystals. *Phys. Rev. B* **67**, 235107 (2003).
35. Cubukcu, E. *et al.* Negative refraction by photonic crystals. *Nature* **423**, 604–605 (2003).
36. Parimi, V. P. *et al.* Imaging by flat lens using negative refraction. *Nature* **426**, 404 (2003).
37. Cubukcu, E. *et al.* Subwavelength resolution in a two-dimensional photonic-crystal-based superlens. *Phys. Rev. Lett.* **91**, 207401 (2003).
38. Li, Z. Y. & Lin, L. L. Evaluation of lensing in photonic crystal slabs exhibiting negative refraction. *Phys. Rev. B* **68**, 245110 (2003).
39. Shvets, G. & Urzhumov, Y. A. Engineering the electromagnetic properties of periodic nanostructures using electrostatic resonance. *Phys. Rev. Lett.* **93**, 243902 (2004).
40. Schonbrun, E. *et al.* Wave front evolution of negatively refracted waves in a photonic crystal. *Appl. Phys. Lett.* **90**, 041113 (2007).
41. Podolskiy, V. A. & Narimanov, E. E. Near-sighted superlens. *Opt. Lett.* **30**, 75–77 (2005).
42. Durant, S. *et al.* Theory of the transmission properties of an optical far-field superlens for imaging beyond the diffraction limit. *J. Opt. Soc. Am. B* **23**, 2383–2392 (2006).
43. Liu, Z. *et al.* Far-field optical superlens. *Nano Lett.* **7**, 403–408 (2007).
44. Liu, Z. *et al.* Experimental studies of far-field superlens for sub-diffractive optical imaging. *Opt. Express* **15**, 6947–6954 (2007).
45. Xiong, Y. *et al.* Tuning the far-field superlens: from UV to visible. *Opt. Express* **15**, 7095–7102 (2007).
46. Xiong, Y., Liu, Z., Sun, C. & Xiang, X. Two-dimensional imaging by far-field superlens at visible wavelengths. *Nano Lett.* **7**, 3360–3365 (2007).
47. Jacob, Z., Alekseyev, L. V. & Narimanov, E. Optical hyperlens: far-field imaging beyond the diffraction limit. *Opt. Express* **14**, 8247–8256 (2006).
48. Salandrino, A. & Engheta, N. Far-field subdiffraction optical microscopy using metamaterial crystals: theory and simulations. *Phys. Rev. B* **74**, 075103 (2006).
49. Lee, H. *et al.* Development of optical hyperlens for imaging below the diffraction limit. *Opt. Express* **15**, 15886–15891 (2007).
50. Pendry, J. B. & Ramakrishna, S. A. Near-field lenses in two dimensions. *J. Phys. Condens. Matter* **14**, 8463–8479 (2002).
51. Pendry, J. B. Perfect cylindrical lenses. *Opt. Express* **11**, 755–760 (2003).
52. Liu, Z. *et al.* Far-field optical hyperlens magnifying sub-diffraction-limited objects. *Science* **315**, 1686 (2007).
53. Smolyaninov, I. I., Huang, Y. J. & Davis, C. C. Magnifying superlens in the visible frequency range. *Science* **315**, 1699–1701 (2007).
54. Drezet, A., Hohenau, A. & Krenn, J. R. Comment on “Far-field optical microscopy with a nanometer-scale resolution based on the in-plane image magnification by surface plasmon polaritons”. *Phys. Rev. Lett.* **98**, 209730 (2007).
55. Zhang, S. *et al.* Experimental demonstration of near-infrared negative-index metamaterials. *Phys. Rev. Lett.* **95**, 137404 (2005).
56. Shalaev, V. M. *et al.* Negative index of refraction in optical metamaterials. *Opt. Lett.* **30**, 3356–3358 (2005).
57. Dolling, G. *et al.* Simultaneous negative phase and group velocity of light in a metamaterial. *Science* **312**, 892–894 (2006).
58. Dolling, G. *et al.* Negative-index metamaterial at 780 nm wavelength. *Opt. Lett.* **32**, 53–55 (2007).
59. Grigorenko, A. N. *et al.* Nanofabricated media with negative permeability at visible frequencies. *Nature* **438**, 335–338 (2005).
60. Grigorenko, A. Negative refractive index in artificial metamaterials. *Opt. Lett.* **31**, 2483–2485 (2006).
61. Liu, Z. Y. *et al.* Locally resonant sonic materials. *Science* **289**, 1734–1736 (2000).
62. Fang, N. *et al.* Ultrasonic metamaterials with negative modulus. *Nature Mater.* **5**, 452–456 (2006).
63. Li, J. & Chan, C. T. Double-negative acoustic metamaterial. *Phys. Rev. E* **70**, 055602 (2004).
64. Yang, S. X. *et al.* Focusing of sound in a 3D phononic crystal. *Phys. Rev. Lett.* **93**, 024301 (2004).
65. Ambati, M. *et al.* Surface resonant states and superlensing in acoustic metamaterials. *Phys. Rev. B* **75**, 195447 (2007).
66. Lu, M. *et al.* Negative birefringence of acoustic waves in a sonic crystal. *Nature Mater.* **6**, 744–748 (2007).
67. Christensen, J. Collimation of sound assisted by acoustic surface waves. *Nature Phys.* **3**, 851–852 (2007).
68. Anker, J. N. *et al.* Biosensing with plasmonic nanosensors. *Nature Mater.* **7**, 442–453 (2008).

Acknowledgements

This work was supported by NSF NSEC award DMI-0327077, ARO MURI award 50432-PH-MUR and AFOSR MURI award FA9550-04-1-0434.